fractal and fractional

MDPI

Article

Numerical and Analytical Study of the Magnetic Field Distribution in a Three-Solenoid System

Mostafa Behtouei [1,*], Alberto Bacci [2], Martina Carillo [1], Moreno Comelli [3], Luigi Faillace [1], Mauro Migliorati [4,5], Livio Verra [1] and Bruno Spataro [1]

[1] Laboratori Nazionale di Frascati, Istituto Nazionale di Fisica Nucleare, Via Enrico Fermi 54, 00044 Frascati, Italy; martina.carillo@uniroma1.it (M.C.); luigi.faillace@lnf.infn.it (L.F.); livio.verra@lnf.infn.it (L.V.); bruno.spataro@lnf.infn.it (B.S.)
[2] Istituto Nazionale di Fisica Nucleare, Sezione di Milano, 20054 Segrate, Italy; alberto.bacci@mi.infn.it
[3] Istituto di Fisica Applicata "Nello Carrara" del Consiglio Nazionale delle Ricerche (CNR-IFAC), Via Madonna del Piano 10, 50019 Sesto Fiorentino, Italy; m.comelli@ifac.cnr.it
[4] Dipartimento di Scienze di Base e Applicate per l'Ingegneria (SBAI), Università degli Studi di Roma "La Sapienza", Via Scarpa 14, 00161 Rome, Italy; mauro.migliorati@uniroma1.it
[5] INFN/Roma1, Istituto Nazionale di Fisica Nucleare, Piazzale Aldo Moro, 2, 00185 Rome, Italy
* Correspondence: mostafa.behtouei@lnf.infn.it

Abstract: This study investigates the magnetic fields produced by a three-solenoid system configuration using both traditional numerical solvers and fractional integral methods. We focus on the role of mesh resolution in influencing simulation accuracy, examining coils with dimensions 80 mm × 160 mm and a radius of 15.5 mm, each carrying a current of 200 A. Magnetic field behavior is analyzed along a line parallel to the central axis at a distance equal to half the solenoid's radius. The fractional integral formulation employed provides a refined understanding of field variations, especially in off-axis regions. Comparisons with the Poisson solver highlight consistency across methods and suggest pathways for further optimization. The results support the potential of fractional approaches in advancing electromagnetic field modeling, particularly in accelerator and beamline applications.

Keywords: magnetic field; solenoid; particle acceleration; linac; accelerator applications; accelerator subsystems and technologies

Academic Editor: Haci Mehmet Baskonus

Received: 23 April 2025
Revised: 4 June 2025
Accepted: 13 June 2025
Published: 16 June 2025

Citation: Behtouei, M.; Bacci, A.; Carillo, M.; Comelli, M.; Faillace, L.; Migliorati, M.; Verra, L.; Spataro, B. Numerical and Analytical Study of the Magnetic Field Distribution in a Three-Solenoid System. *Fractal Fract.* **2025**, *9*, 383. https://doi.org/10.3390/fractalfract9060383

1. Introduction

Accurate modeling of magnetic fields in solenoid systems with multiple coils is essential for the design and optimization of advanced electromagnetic devices. The ability to precisely determine magnetic fields in solenoids and coils plays a central role in many areas of applied physics and engineering. These field components are fundamental in the development of particle accelerators such as high-brilliance photoinjectors and high-gradient accelerating structures as well as in magnetic correctors and steering systems used to align particle beams. A key challenge in these applications is the control and stabilization of beam trajectories, particularly in the presence of space charge effects [1–5]. In this work, we examine a system composed of three coils, exploring how mesh resolution impacts numerical accuracy. This study analyzes the magnetic field behavior in off-axis positions using the Poisson solver [6]. Our goal is to validate the numerical models and quantify potential errors arising from different mesh configurations.

The theoretical basis for calculating magnetic fields generated by current-carrying conductors is well established. At its core lies the Biot–Savart law, a direct consequence of Maxwell's equations, which provides a powerful tool for evaluating magnetic fields from a

given current distribution [7]. This law has enabled analytical solutions for idealized cases such as thin wires, loops, and infinite solenoids. However, when dealing with more realistic geometries like solenoids of finite length or conductors with distributed surface currents, the problem becomes considerably more complex and often requires numerical approaches.

Over the years, several researchers have proposed methods to overcome these challenges. For example, Bassetti et al. [8] developed an analytical model for the near-axis magnetic potential of multipole configurations, which relied heavily on numerical techniques to handle higher-order terms when moving away from the axis. Similarly, Caciagli et al. [9] derived analytical expressions for the magnetic field of finite-length cylinders with uniform transverse magnetization using complete elliptic integrals. Despite the progress, the presence of fractional integrals of orders $3/2$ and $1/2$ in these formulations introduced mathematical complications, such as branch lines, which required special attention in the computations.

In our previous work [10,11], we tackled these difficulties by analyzing solenoids composed of discrete coils and introduced an innovative method to address the issue of branch lines in fractional integrals. We later extended this approach to solenoids formed by continuous conductive sheets, using surface current density distributions to derive the corresponding magnetic fields [10].

We begin by analyzing the magnetic field produced by a single thin coil of radius R, evaluating its intensity both along the axis and at various off-axis locations. We then apply the superposition principle to construct the field of a complete solenoid. Through a detailed comparison between analytical and numerical solutions, we aim to provide a deeper understanding of the field characteristics across different configurations.

By integrating theory and simulations, this study offers a comprehensive framework for accurately determining magnetic fields in solenoids. The results have significant implications for accelerator physics, beam dynamics, and the design of magnetic devices in cutting-edge scientific and technological applications.

This work aims to expand on these methodologies by applying fractional integral techniques to a three-solenoid system. We examine how variations in mesh resolution affect numerical accuracy and convergence, and compare results obtained from a Poisson solver with those from our fractional approach. Through this comparative study, we aim to validate the robustness of the fractional method and provide insight into optimization strategies for electromagnetic simulations.

Although the analytical solution, combined with the superposition principle, provides an exact calculation for the magnetic field of the idealized coil system studied, numerical solutions of the Poisson equation remain essential. Numerical methods offer greater flexibility for handling more complex geometries and realistic boundary conditions where analytical solutions may not be available. Additionally, the numerical solver acts as an independent tool for validating and benchmarking the analytical fractional integral approach, thereby increasing confidence in the results. This comparison also guides mesh optimization and error estimation, which are critical for ensuring accuracy in practical computational scenarios.

2. Analytical Method

The fractional integral method, which emerges from fractional calculus, extends classical integral operators to non-integer orders, offering enhanced flexibility to describe complex physical phenomena. In the context of electromagnetic field modeling, this approach provides a powerful mathematical framework capable of capturing subtle spatial variations and memory effects that traditional integer-order formulations may overlook.

Introducing fractional integrals here lays the groundwork for applying this innovative method to the magnetic field calculations of the studied solenoid system.

Alongside this, magnetic fields in solenoids and coil systems have traditionally been determined through well-established analytical expressions. In this section, we first review these key classical formulas for magnetic field components across various coil configurations, establishing a solid foundation that supports and complements the fractional integral formulation and subsequent numerical analyses presented later in the work.

2.1. Magnetic Field for a Single Thin Coil

For a single thin circular coil of radius R, carrying a steady current I, the magnetic field components can be derived using the Biot–Savart law. We adopt a cylindrical coordinate system (r, ϕ, z), where the origin is placed at the center of the coil, which lies in the x-y plane (i.e., at $z = z_0$). The axis of the coil is aligned with the z-axis.

The resulting expressions for the radial ($\mathbf{B_r}$) and axial ($\mathbf{B_z}$) components of the magnetic field at an arbitrary point in space are given by [10]

$$\mathbf{B}_r = \frac{\mu_0 I M_z}{2R}\left(\frac{\xi}{2\eta(1+\xi)}\right)^{3/2}\left[{}_2F_1\left(\frac{3}{2},\frac{3}{2};2;\frac{2\xi}{1+\xi}\right) - {}_2F_1\left(\frac{1}{2},\frac{3}{2};1;\frac{2\xi}{1+\xi}\right)\right], \quad (1)$$

$$\mathbf{B}_z = \frac{\mu_0 I}{2R}\left(\frac{\xi}{2\eta(1+\xi)}\right)^{3/2}\left[(1+\eta)\,{}_2F_1\left(\frac{1}{2},\frac{3}{2};1;\frac{2\xi}{1+\xi}\right) - \eta\,{}_2F_1\left(\frac{3}{2},\frac{3}{2};2;\frac{2\xi}{1+\xi}\right)\right], \quad (2)$$

where

- μ_0 is the permeability of free space;
- I is the current through the coil;
- R is the radius of the coil;
- r is the radial distance of the observation point from the axis of the coil;
- z is the axial distance of the observation point from the origin;
- z_0 is the axial coordinate of the coil center;
- $M_z = \frac{z-z_0}{R}$ is the normalized axial distance from the coil plane;
- $\eta = \frac{r}{R}$ is the normalized radial coordinate;
- ${}_2F_1(a, b; c; z)$ denotes the Gaussian hypergeometric function.

The dimensionless geometric parameter ξ, which governs the field configuration based on the relative positions of the observation point and the coil, is defined as

$$\xi(r, R, z) = \frac{2rR}{r^2 + R^2 + (z - z_0)^2}. \quad (3)$$

This formulation enables precise evaluation of magnetic fields both on and off the symmetry axis of the coil.

2.2. Magnetic Field for Finite-Length Solenoids

For a solenoid of finite length, the magnetic field becomes more intricate due to the continuous distribution of current along the axial direction. To model this, we use a cylindrical coordinate system (r, ϕ, z), where the solenoid is aligned along the z-axis and centered at $z = z_0$. Assuming a uniform surface current density K flowing azimuthally over the solenoid surface, the magnetic field components at any observation point (r, z) can be obtained by integrating the contributions of individual circular current loops along the solenoid length [11].

The normalized radial and axial coordinates are defined as $\eta = \frac{r}{R}$ and $M_z = \frac{z-z_0}{R}$, respectively, where R is the radius of the solenoid and z_0 is the axial position of its center.

The half-length of the solenoid is normalized as $M_{z_\ell} = \frac{L}{2R}$, where L is the total length of the solenoid.

The radial and axial components of the magnetic field, $\mathbf{B_r}$ and $\mathbf{B_z}$, are given by

$$\mathbf{B}_r = \frac{\mu_0 K}{2} \int_{\sqrt{(1+\eta)^2+(M_z-M_{z_\ell})^2}}^{\sqrt{(1+\eta)^2+(M_z+M_{z_\ell})^2}} \frac{1}{\beta^2} \left[{}_2F_1\left(\frac{1}{2}, \frac{3}{2}; 1; \frac{4\eta}{\beta^2}\right) - {}_2F_1\left(\frac{3}{2}, \frac{3}{2}; 2; \frac{4\eta}{\beta^2}\right) \right] d\beta, \quad (4)$$

$$\mathbf{B}_z = \frac{-\mu_0 K}{2} \int_{\sqrt{(1+\eta)^2+(M_z-M_{z_\ell})^2}}^{\sqrt{(1+\eta)^2+(M_z+M_{z_\ell})^2}} \frac{1}{\beta^2 \sqrt{\beta^2-(1+\eta)^2}} \left[{}_2F_1\left(\frac{1}{2}, \frac{3}{2}; 1; \frac{4\eta}{\beta^2}\right) + \eta \left({}_2F_1\left(\frac{1}{2}, \frac{3}{2}; 1; \frac{4\eta}{\beta^2}\right) - {}_2F_1\left(\frac{3}{2}, \frac{3}{2}; 2; \frac{4\eta}{\beta^2}\right) \right) \right] d\beta. \quad (5)$$

In these expressions

- K is the surface current density on the solenoid;
- $M_{z_\ell} = \frac{L}{2R}$ is the normalized half-length of the solenoid;
- β is an integration variable associated with the distance from the observation point to the elemental current ring.

These integrals account for the cumulative magnetic field contributions from all elemental current loops making up the solenoid. The resulting expressions serve as a benchmark for validating the numerical simulations discussed in the subsequent sections.

3. Comparison Between Numerical Simulations and Analytical Results

The layout and design of the three coils used in this study are illustrated in Figure 1, showing the geometric configuration and structural considerations [12]. Each coil is designed with a rectangular cross-section measuring 80 mm by 160 mm. The coils are constructed with 10 longitudinal layers and 20 radial layers, each made from square wire segments with dimensions of 7.5 mm by 7.5 mm. To ensure efficient cooling during high-current operations, each wire segment is equipped with a central hole of 5 mm diameter, facilitating coolant circulation through the coil. Moreover, a 0.5 mm gap is maintained between adjacent wire segments to provide insulation, helping to minimize thermal stress and maintain the structural integrity of the coils.

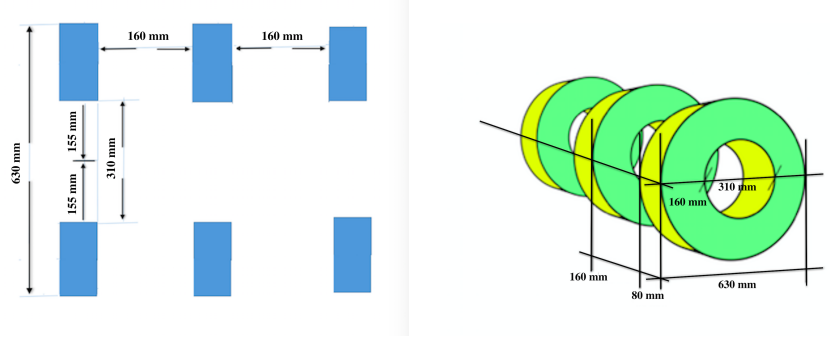

(**a**) (**b**)

Figure 1. (**a**) Schematic layout of the three-spool solenoid configuration. Each spool has a width of 80 mm and a height of 160 mm, with a vertical spacing of 155 mm between adjacent spools. The total height of the solenoid system is 630 mm. (**b**) Three-dimensional rendering of the solenoid configuration. The horizontal distance between neighboring solenoids is 160 mm, and the central solenoid is positioned symmetrically between the two outer ones.

The coils are arranged symmetrically in a rectangular layout, with a vertical separation of 155 mm and horizontal spacing of 160 mm. This results in a total system height of 630 mm and a width of 310 mm. This configuration not only ensures a uniform magnetic field distribution but also integrates essential thermal management features to support the coils' operation at a total current of 40 kA each. The design effectively combines efficiency and reliability, making it suitable for high-power applications.

Magnetic field simulations for this coil system was carried out using the Poisson solver, both of which are highly effective for modeling electromagnetic systems with high precision. The simulations were performed using the different mesh resolutions 200 µm, 300 µm, 400 µm, 500 µm, and 600 µm to ensure that field dynamics were captured accurately while balancing computational resource usage. Within the winding regions of the coils, a uniform and fine mesh ($dx = dy$) was used to achieve high resolution where magnetic field gradients are expected to be most significant. In contrast, a coarser mesh was applied outside the coils, where magnetic field variations are less critical, allowing for reduced computational overhead without sacrificing overall simulation accuracy.

This combination of fine and coarse meshing strategies provides a reliable method for balancing computational efficiency with the need for detailed electromagnetic analysis. The results from these simulations were compared against theoretical predictions to assess the accuracy of the field distribution.

Magnetic field simulations are essential for the design and analysis of electromagnets and solenoids, particularly when aiming to balance numerical accuracy with computational efficiency. This section examines the trade-off between these two factors, specifically focusing on the accuracy of magnetic field calculations obtained through the Poisson solver.

Figure 2 presents the analytical and numerical results of the magnetic field generated by a solenoid composed of three spools. Figure 2a shows the magnetic field components, both axial and radial, at an off-axis distance of 0.5 R (R = 155 mm), obtained through analytical methods. Figure 2b presents the corresponding magnetic field components at the same off-axis distance derived from Poisson software, Version 7.0. Figure 2c depicts the magnetic field lines of the solenoid, as simulated by Poisson software, offering a visual representation of the field's direction and intensity across the solenoid's structure.

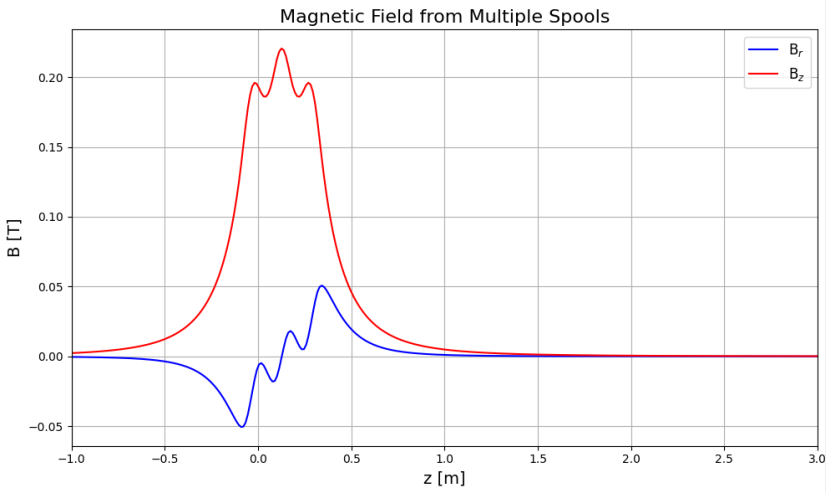

(**a**)

Figure 2. *Cont.*

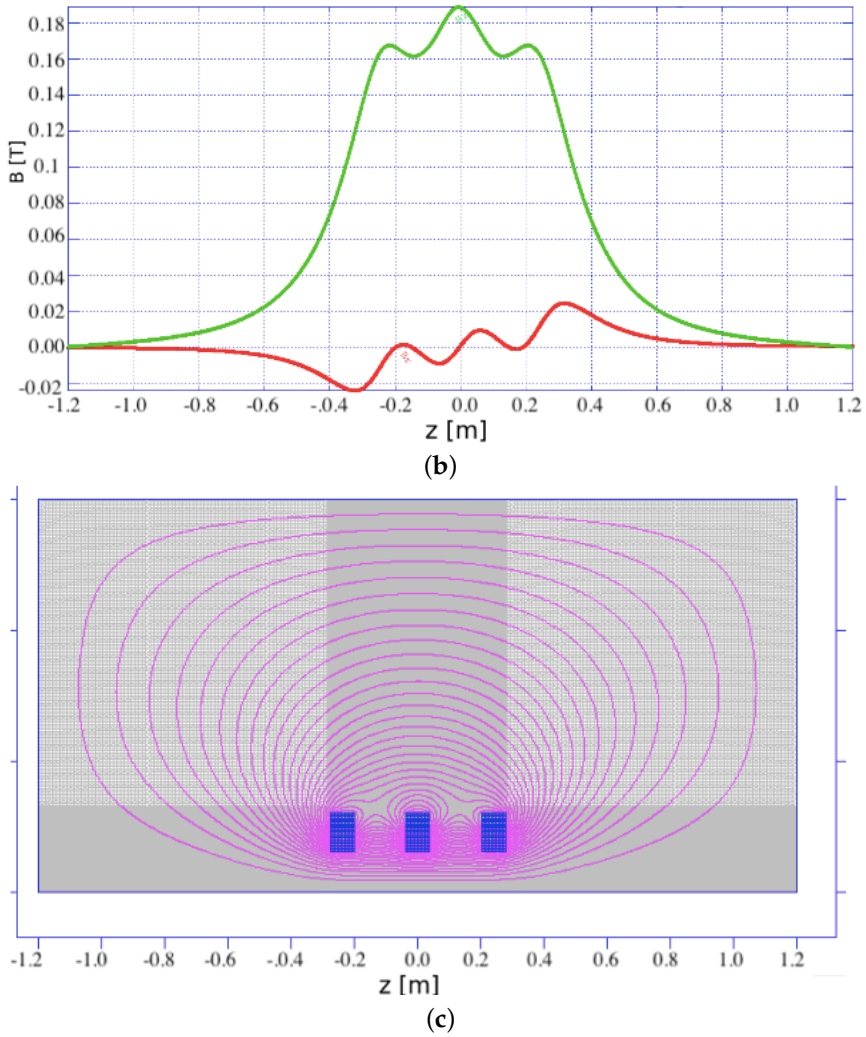

Figure 2. Analytical and numerical results of the axial and radial magnetic field generated by three-solenoid spools at an off-axis distance of 0.5 R. (**a**) Analytical magnetic field results. (**b**) Simulations results obtained using Poisson software. (**c**) Magnetic field lines of the solenoid, simulated using Poisson software.

Figure 3 shows a comparison between analytical and numerical results. Figure 3a presents the axial magnetic field using a coil radius of 155 mm, with different mesh sizes in simulations compared to the analytical solution. The small plot in the corner helps to better see the differences near the center of the structure. Figure 3b shows a similar comparison for the axial magnetic field, but using an average coil radius of 235 mm, which represents the average radius of the solenoid's coils [13]. The results still show good agreement between the two methods. Figure 3c shows the radial magnetic field for the average coil radius of 235 mm, comparing numerical and analytical results using a 200 µm mesh size. The graph shows how the radial field changes near the edges of the solenoid. While the axial magnetic field obtained from numerical simulations closely matches the analytical solution, the radial component exhibits a significant discrepancy by a factor of approximately 2, when comparing the two methods. This difference is likely due to the increased sensitivity of the radial field to geometric approximations and edge effects inherent in the numerical model, as discussed by Fleurot et al. [14].

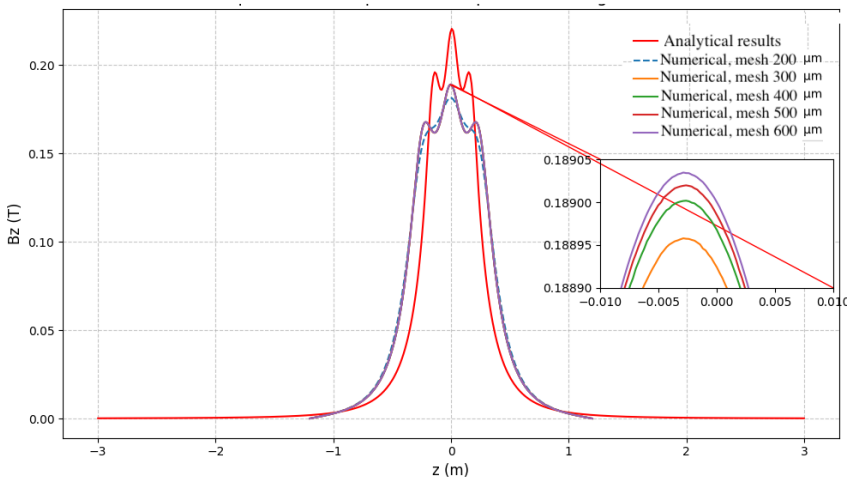

(**a**)

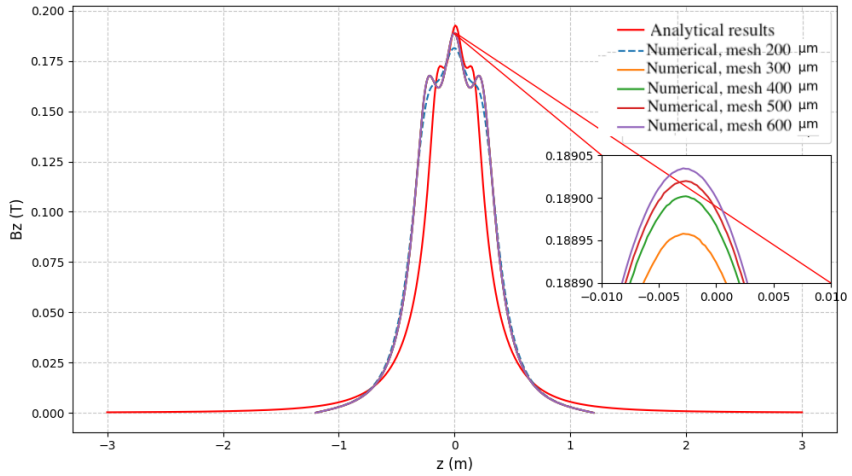

(**b**)

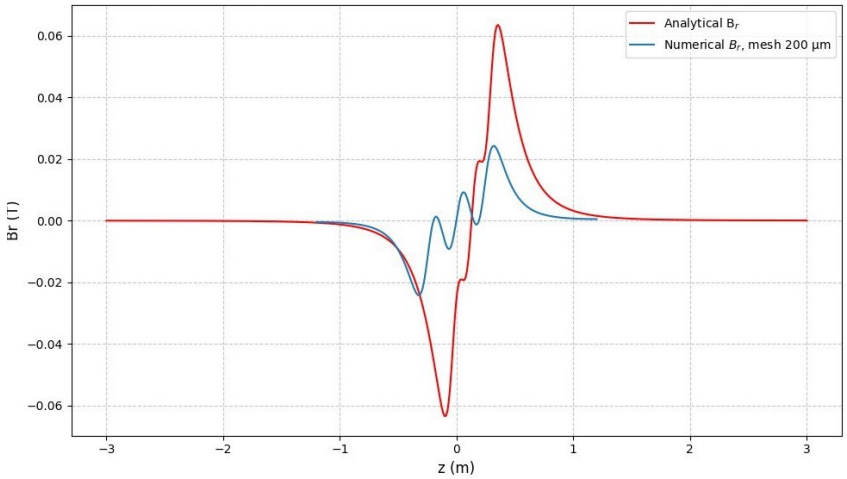

(**c**)

Figure 3. Comparison of analytical and numerical magnetic field results for the three-solenoid spools. (**a**) Axial field with coil radius 155 mm. (**b**) Axial field with average radius 235 mm. (**c**) Radial field with average radius 235 mm and 200 μm mesh size.

The mesh resolution plays a crucial role in determining the accuracy of the magnetic field simulations. A finer mesh improves the precision of the results but increases the computational cost, while a coarser mesh reduces the computational time but may intro-

duce errors. Table 1 summarizes the peak magnetic field values $\mathbf{B_z}$ and corresponding computation times for the various mesh resolutions tested in this study.

Table 1. Peak magnetic field values and computation times for different mesh resolutions.

Mesh Size (µm)	Peak B_z (G)	Computation Time (h:min)
200	1889.6	4:00
300	1890.0	2:30
400	1890.2	1:30
590	1890.4	0:30

As shown in Table 1, the differences in peak $\mathbf{B_z}$ values across the mesh resolutions are minimal, with a maximum deviation of less than 0.05%. This demonstrates the numerical stability of the solver, even with varying mesh sizes. While the computational time decreases significantly with coarser meshes, the (590 µm) mesh offers the most efficient balance, providing results comparable to those from finer meshes but at a fraction of the computational cost.

To further assess numerical accuracy, the relationship between mesh resolution and the magnetic field estimations $\mathbf{B_z}$ was analyzed. Figure 4b presents a second-degree polynomial fit of the form

$$Y = M_0 + M_1 x + M_2 x^2,$$

where x represents the mesh resolution parameter (i.e., the number of mesh elements used in the simulation), and the coefficients are given by $M_0 = 1888.6$, $M_1 = 0.0063478$, and $M_2 = -5.4859 \times 10^{-6}$. The high coefficient of determination ($R = 0.99793$) reflects an excellent fit to the data, with the maximum error between the actual data and the polynomial estimation being less than 0.003%. This demonstrates the robustness of the polynomial model and validates its use for approximating field behavior as a function of mesh size.

Figure 4a shows the same data fitted using a third-degree polynomial. This model captures the slight nonlinear behavior more effectively as the mesh becomes finer, resulting in an even better fit with a correlation coefficient of $R = 1$. The third-degree polynomial, shown in Figure 4a, thus provides a more precise approximation, especially when the changes in the magnetic field are not perfectly smooth. Together, the two fits confirm the consistency and accuracy of the numerical approach across different polynomial models and mesh resolutions.

The numerical error is defined as the difference between the numerical solution $\mathbf{B}_h$ and the exact solution $\mathbf{B}_{\text{exact}}$, with the error function given by

$$\text{Error}_{L_2}(h) = \sqrt{\int_\Omega \|\mathbf{B}_h - \mathbf{B}_{\text{exact}}\|^2 \, d\Omega},$$

where Ω is the computational domain and h is the mesh size. The error inside the solenoid is given by [15]

$$\text{Error}_{\text{inside}} = Ch^p \sqrt{\pi R^2},$$

where R is the solenoid radius, and the error outside the solenoid is negligible because the exact magnetic field is nearly zero, making the numerical error minimal. Thus, its contribution to the total L_2 norm error is insignificant compared to the inside. The total error is dominated by the contribution inside the solenoid, and it scales as $\text{Error}_{L_2}(h) \propto h^p$,

indicating that smaller mesh sizes or higher-order numerical methods are needed for higher accuracy [15,16].

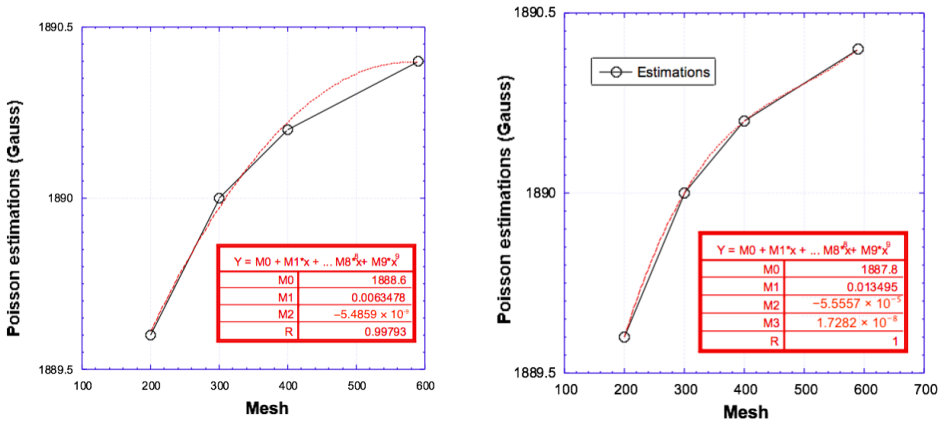

(**a**) (**b**)

Figure 4. Comparison of numerical estimations of $\mathbf{B_z}$ for different mesh sizes, including polynomial error fitting. (**a**) Poisson field estimations $\mathbf{B_z}$ as a function of mesh size, with a polynomial fit for error analysis. (**b**) Poisson field estimations $\mathbf{B_z}$ as a function of mesh size, analyzed with a second-degree polynomial fit for error estimation. The approximation error is shown to be less than 0.003%. Note: The asterisk (*) in the figure denotes multiplication.

The agreement between the Poisson and analytical method further validates the reliability of the simulations. Future work could investigate advanced solver algorithms or adaptive mesh refinement techniques to further enhance accuracy while reducing computational costs.

Although the main emphasis of this section lies in comparing numerical and analytical results using conventional methods, it is important to highlight that the discrepancies observed—particularly in the radial magnetic field component—indicate the limitations of classical integer-order models in capturing complex geometrical and boundary-induced variations. This observation motivates the potential application of fractional integral methods, which generalize classical calculus to non-integer orders and offer an enriched mathematical framework capable of incorporating memory effects, nonlocal interactions, and spatial heterogeneities. While not yet fully implemented in this numerical stage, the inclusion of fractional calculus concepts—introduced in the abstract and discussed in the conclusion—provides a promising direction for refining field models beyond the capabilities of traditional methods. In future work, the framework established here will serve as a foundation for integrating fractional approaches to enhance accuracy, particularly in regions where standard models show measurable deviations.

4. Conclusions

This study demonstrates the effectiveness and high accuracy of magnetic field simulations for a three-solenoid system, with particular attention to mesh resolution and its impact on numerical precision. Across various mesh sizes, the results show that the numerical error remains exceptionally low, with variations in the peak axial magnetic field $\mathbf{B_z}$ staying below 0.05%. This confirms that reliable and accurate simulations are achievable even with coarser meshes, offering a significant computational advantage.

Moreover, the close agreement between the Poisson solver results and the fractional integral formulation underscores the robustness of the analytical approach. The fractional method, in particular, provides a powerful alternative to conventional techniques, especially in off-axis regions where classical models often face limitations. These findings highlight

the potential of fractional calculus as a complementary framework for electromagnetic field modeling, combining analytical flexibility with computational efficiency.

While the current analysis focuses on a specific three-solenoid configuration with fixed dimensions and coil spacing, the proposed fractional integral methodology is generalizable to similar coil systems with varying geometries, provided the fundamental assumptions of axial symmetry and boundary conditions are preserved. This adaptability makes the approach promising for a broader range of magnetic field modeling applications in accelerator and beam line design.

In addition, our comparison between analytical and numerical techniques showed that mesh resolution plays a critical role in simulation accuracy. As expected, finer meshes improve precision but increase computational cost. However, using polynomial fitting techniques, we verified that the numerical error can be minimized below 0.003% with optimized mesh choices. These results offer practical recommendations for balancing accuracy and computation time.

In summary, the study offers practical insights into mesh resolution optimization while validating fractional integral methods as a precise and reliable tool for magnetic field analysis in complex solenoid configurations.

Author Contributions: Conceptualization, M.B. and B.S.; methodology, M.B. and B.S.; software, M.B., A.B., M.C. (Martina Carillo), M.C. (Moreno Comelli) and L.V.; validation, M.B., M.C. (Moreno Comelli), L.F., M.M. and B.S.; formal analysis, M.B.; investigation, M.B. and B.S.; data curation, M.B.; writing original draft preparation, M.B.; writing, review and editing, M.B.; visualization, M.B.; supervision, L.F., M.M. and B.S.; project administration, M.M. and B.S. All authors have read and agreed to the published version of the manuscript.

Funding: This research received no external funding.

Data Availability Statement: All data can be made available on request.

Conflicts of Interest: The authors declare no conflicts of interest.

References

1. Ferrario, M.; Alesini, D.; Bacci, A.; Bellaveglia, M.; Boni, R.; Boscolo, M.; Castellano, M.; Catani, L.; Chiadroni, E.; Cialdi, S.; et al. Direct measurement of the double emittance minimum in the beam dynamics of the SPARC high-brightness photoinjector. *Phys. Rev. Lett.* **2007**, *99*, 234801. [CrossRef] [PubMed]
2. Migliorati, M.; Dattoli, G. Transport matrix of a solenoid with linear fringe field. *Il Nuovo C. Della Societá Ital. Fisica-B Gen. Phys. Relativ. Astron. Math. Phys. Methods* **2009**, *124*, 385.
3. Nezhevenko, O.A.; Yakovlev, V.P.; Hirshfield, J.L.; Serdobintsev, G.V.; Schelkunoff, S.V.; Persov, B.Z. 34.3 GHz accelerating structure for high gradient tests. In *Proceedings of the PACS2001. Proceedings of the 2001 Particle Accelerator Conference (Cat. No. 01CH37268), Chicago, IL, USA, 18–22 June 2001;* IEEE: Chicago, IL, USA; Volume 5.
4. Behtouei, M.; Faillace, L.; Ferrario, M.; Spataro, B.; Variola, A. Initial design of a high-power Ka-band klystron. *arXiv* **2020**, arXiv:2002.04873. [CrossRef]
5. Behtouei, M.; Spataro, B.; Paolo, F.D.; Leggieri, A. The Ka-band high power klystron amplifier design program of INFN. *Vacuum* **2021**, *191*, 110377. [CrossRef]
6. McKenney, A.; Greengard, L.; Mayo, A. A fast Poisson solver for complex geometries. *J. Comput. Phys.* **1995**, *118*, 348–355. [CrossRef]
7. Jackson, J.D. *Classical Electrodynamics*; Springer: New York, NY, USA, 1999; pp. 841–842.
8. Bassetti, M.; Biscari, C. Analytical formulae for magnetic multipoles. *Part. Accel.* **1996**, *52*, 221–250.
9. Caciagli, A.; Baars, R.J.; Philipse, A.P.; Kuipers, B.W. Exact expression for the magnetic field of a finite cylinder with arbitrary uniform magnetization. *J. Magn. Magn. Mater.* **2018**, *456*, 423–432. [CrossRef]
10. Behtouei, M.; Faillace, L.; Spataro, B.; Variola, A.; Migliorati, M. A Novel Exact Analytical Expression for the Magnetic Field of a Solenoid. *arXiv* **2020**, arXiv:2002.09444. [CrossRef]
11. Behtouei, M.; Spataro, B.; Faillace, L.; Carillo, M.; Comelli, M.; Variola, A.; Migliorati, M. A novel method to calculate the magnetic field of a solenoid generated by a surface current element. *arXiv* **2022**, arXiv:2109.04464. [CrossRef]
12. Vannozzi , A. (INFN-LNF, Frascati, Italy). Private communication, 2022.

13. Lyle, T.R. Xxxii. on circular filaments or circular magnetic shells equivalent to circular coils, and on the equivalent radius of a coil. *Lond. Edinb. Dublin Philos. Mag. J. Sci.* **1902**, *3*, 310–329. [CrossRef]
14. Fleurot, E.; Scuiller, F.; Charpentier, J. Analytical models for fast and accurate calculation of electromagnetic performances of segmented permanent magnet synchronous machines with large angular gaps. *Appl. Sci.* **2021**, *11*, 459. [CrossRef]
15. Klaus-Jurgen Bathe. *Finite Element Procedures*; Klaus-Jurgen Bathe: Cambridge, MA, USA, 2006.
16. Reddy, J.N. *Introduction to the Finite Element Method*, 4th ed.; Springer: Berlin/Heidelberg, Germany, 2019.